






Article

Poly(Lactic Acid) (PLA)-Based Nanocomposites: Impact of Vermiculite, Silver, and Graphene Oxide on Thermal Stability, Isothermal Crystallization, and Local Mechanical Behavior

Sabrine Khammassi ^{1,*} , Mostapha Tarfaoui ^{1,2,*} , Kateřina Škrlová ^{3,4}, Dagmar Měřínská ⁵ , Daniela Plachá ^{3,6,*}  and Fouad Erchiqui ⁷ 

¹ ENSTA BretAgne, IRDL-UMR CNRS 6027, F-29200 Brest, France

² Green Energy Park (IRESEN/UM6P), km2 R206, Benguerir 43150, Morocco

³ Nanotechnology Centre, CEET, VSB—Technical University of Ostrava, 17. Listopadu 2172/15, 708 00 Ostrava, Czech Republic; katerina-skrlova@vsb.cz

⁴ Center of Advanced Innovation Technologies, VSB—Technical University of Ostrava, 17. Listopadu 2172/15, 708 00 Ostrava, Czech Republic

⁵ Faculty of Technology, Tomas Bata University in Zlín, Vavrečkova 275, 760 01 Zlín, Czech Republic; merinska@utb.cz

⁶ ENET Centre, CEET, VSB—Technical University of Ostrava, 17. Listopadu 2172/15, 708 00 Ostrava, Czech Republic

⁷ Campus de Rouyn-Noranda, 445, Université du Québec en Abitibi-Témiscamingue, Rouyn-Noranda, QC J9X 5E4, Canada; fouad.erchiqui@uqat.ca

* Correspondence: sabrine.khammassi@ensta-bretAgne.org (S.K.);

mostapha.tarfaoui@ensta-bretAgne.org (M.T.); daniela.placha@vsb.cz (D.P.)



Citation: Khammassi, S.; Tarfaoui, M.; Škrlová, K.; Měřínská, D.; Plachá, D.; Erchiqui, F. Poly(Lactic Acid) (PLA)-Based Nanocomposites: Impact of Vermiculite, Silver, and Graphene Oxide on Thermal Stability, Isothermal Crystallization, and Local Mechanical Behavior. *J. Compos. Sci.* **2022**, *6*, 112. <https://doi.org/10.3390/jcs6040112>

Academic Editors: Thanasis Triantafyllou and Francesco Todaro

Received: 13 February 2022

Accepted: 30 March 2022

Published: 8 April 2022

Publisher's Note: MDPI stays neutral with regard to jurisdictional claims in published maps and institutional affiliations.



Copyright: © 2022 by the authors. Licensee MDPI, Basel, Switzerland. This article is an open access article distributed under the terms and conditions of the Creative Commons Attribution (CC BY) license (<https://creativecommons.org/licenses/by/4.0/>).

Abstract: The structural, thermal, and mechanical properties of unreinforced and reinforced polylactic acid (PLA) were investigated. The PLA was a biopolymer that was reinforced with four fillers (i.e., graphene oxide (GO) and silver (Ag); vermiculite (VMT) and silver (Ag); and two organically modified vermiculites). The processing technique for the production of the composite materials were carefully planned. The PLA nanocomposites were investigated by examining their morphological aspects, changes in PLA phases and transitions and, most importantly, the effect on certain final properties. X-ray diffraction and differential scanning calorimetry (DSC) analysis indicated that the sample was completely amorphous. Thermogravimetric analysis (TGA) results indicated that the presence of reinforcing particles in the PLA matrix did not affect the thermal degradation of these composites. Furthermore, the local mechanical properties were investigated using the microindentation method to evaluate the effect of different nanofillers. Scanning electron microscopy (SEM) and a VHX-500 optical digital microscope (Keyence International, Mechelen, Belgium) were also used to examine the surface morphology of the PLA polymer composites. These results can help to select suitable fillers to enhance the PLA performance of biopolymers.

Keywords: polylactide; composites; thermal stability; isothermal crystallization; microindentation

1. Introduction

Biodegradable polymer composites are widely used in food packaging and agricultural films and have applications in many fields such as artificial joints, wound treatment, related drug delivery, and orthopedic devices.

Poly(lactic acid) (PLA) is a biobased polymer that has recently gained popularity due to its good properties, processability, and relative high availability compared to other commercially used biodegradable thermoplastic polyesters [1–3].

Poly(lactic acid) (PLA) is polyester with high strength and biocompatibility that is widely used in biomedical applications [4–8]. PLA is a biodegradable material made from renewable resources. It is cost-effective and can be used for 3D printing. In an amorphous

state, it is light and transparent, has high rigidity, and can be used in contact with food in a variety of thicknesses. It acts as a barrier to fat, oil, odor, and water, and it has a low-sealing temperature [9].

As per some research, many hydrolytic degradation tests on PLA have been executed to simulate its compatibility with the human body and natural sites such as soil or compost [10–12]. PLA is a transparent, glossy, rigid polymer made up of semi-crystalline polymers with glass transition and melting temperatures of approximately 55 and 180 °C, respectively [13,14]. PLA, as some analyses have shown, has many benefits that make it a popular polymer, but it also has some disadvantages that limit its use significantly. Susceptibility to hydrolytic degradation during melt processing, high brittleness, and a low glass transition temperature are among them. Furthermore, according to some sources, PLA is hydrolyzed and produces water-soluble oligomers. PLA's critical degradation rate has limited its use, and several scientists have tried to prove the degradation rate (often to increase speed) and improve PLA for biomedical or environmental applications [1,4,15]. Neat PLA has many limitations in packaging applications, such as food packaging materials, where nanocomposites must have effective antioxidant activity against many human pathogenic bacteria [16–19].

Therefore, as a result, the addition of inorganic and organic nanofillers and nanohybrids is thought to be an appropriate alternative for overcoming these issues, thereby increasing the possibility of PLA-based packaging materials [20,21]. The preparation of reactive blends of polylactide with other biodegradable polymers [15,22] is another solution that allows for the expansion of the field of application, primarily in terms of improving toughness. The use of inorganic fillers in the fabrication of PLA-based composites has created numerous opportunities for modification, leading to the polymer's widespread use [23]. Fillers can change the crystal structure; improve thermomechanical properties [24], thermal conductivity [25], and barrier properties [26]; reduce flammability [27]. Furthermore, when fibrous fillers, such as glass or basalt fibers, were used, the mechanical properties improved significantly [28,29].

Furthermore, Wu et al. [30] confirmed that the viscoelasticity of PLA polymers could be increased by including nanofillers as reinforcement. Viscoelasticity is closely related to the dispersion state of the nanofillers and the interaction between the nanofillers and the polymer matrix. Therefore, elastic and viscosity trends are considered separately to highlight their contributions. However, elastic and viscous behaviors are intrinsically linked and often cannot be separated. For this reason, choosing a good, efficient nanofiller has a powerful impact [31].

Among numerous nanofillers [32–35], vermiculite (VMT), silver (Ag), and graphene oxide (GO) nanofillers are operational in improving the physical properties and crystallization of PLA owing to their excellent physical properties, comprising their high aspect ratio and imperative surface area [36–40].

Silver (Ag) nanoparticles are known to improve the antimicrobial properties of polymeric materials and are widely used as an antimicrobial additive in food applications. Silver nanoparticles (Ag) have also received a lot of attention in biomedical and food packaging products due to the fact of their optical, antibacterial, and thermal properties as well as their very large surface area. Because of the enhancement of antibacterial, antifungal, and antiviral activity of Ag at the nanoscale, Ag nanoparticles are effective against bacteria and can destroy 650 different types of bacteria, viruses, and fungi [41–43]. When compared to other antibacterial agents, these nanoparticles are more durable, effective, and simple to use.

Vermiculite (VMT) is a type of clay that can be used to strengthen polymers. VMT is a layered silicate of the mica type. VMT is a silicate that is more plentiful, less expensive and has a higher cation exchange capacity. Zhang et al. [44] used microwave-assisted in situ polymerization to create PLA/vermiculite nanocomposites. Vermiculite's effect on the emulsion effect and material properties was investigated. Ye et al. [45] used a twin-screw extruder to melt blend poly-L-lactide (PLLA)/vermiculite primary nanocomposites

and investigate the diffusion state of vermiculite as well as the effect of vermiculite on its thermodynamic properties.

Graphene oxide (GO) has incredible properties such as high mechanical strength and a very large surface area [46]. Several studies have been conducted to investigate the enhancement of PLA by GO [47]. Pinto et al. demonstrated that the addition of GO increased the elastic modulus by 115% and the yield strength by 95% [48]. Other research has found that biopolymer-based GO reinforcements are biocompatible, promote cell adhesion and proliferation, and improve composite wettability [38,46,47,49–51].

Other research has found that biopolymer-based GO reinforcements are biocompatible, promote cell adhesion and proliferation, and improve composite wettability [16,21].

Several studies on the micro indentation [32,52] of injection-molded polymers indicate that crystallinity influences both modulus and hardness [53,54]. According to several research works, a good dispersion of nanofillers in the matrix is very important. To reach a good and uniform dispersion, a limited mass fraction of nanofillers must be added to avoid Agglomeration and high density in the reinforced PLA [55]. Thus, the molded polymers could experience uneven cooling rates between the outer and inner parts. Consequently, the amplified crystallization rate stimulated by the integration of vermiculite (VMT), silver (Ag), and graphene oxide (GO) may affect surface properties. The addition of vermiculite (VMT), silver (Ag), and graphene oxide (GO) into PLA leads to a rise in the complex viscosity, storage modulus, and loss modulus, which is more prominent in the low-frequency range than the high-frequency range. This indicates that the reinforced PLA nanocomposites are more elastic than neat PLA, which can lead to the hesitation effect cited above in the micro-injection molding process.

The main idea and novelty of this work were to produce PLA-based nanocomposites reinforced with nanofillers by extrusion and to evaluate their thermal stability, crystallization ability, and mechanical response (under different solicitation or isothermal conditions). The nanofillers used in this work are known to have antimicrobial properties. The PLA used was PLA designed for 3D printing due to the intended future applications. Hence, on the following nanocomposites after extrusion, we focused on the morphological aspects revealed as well as the effects of the interaction between the PLA matrix and the nanofillers. Many techniques are critical to this study, including transmission electron microscopy (TEM), scanning electron microscopy (SEM), X-ray diffraction analysis, thermogravimetric analysis (TGA), differential scanning calorimetry (DSC), and micro indentation test. The purpose of this study was to investigate the effect of different nanoparticles on the thermal, mechanical, and barrier properties of PLA polymer matrices. The funding contributed to selecting the adequate reinforced nanocomposite to use for various biomedical applications as well as the packaging materials and materials for 3D printing.

2. Materials and Methods

2.1. Materials

Granular polylactide (PLA) of a technical grade mainly used for 3D printing was supplied by Plasty Mladeč, Czech Republic (density of $1.24 \text{ g}\cdot\text{cm}^{-3}$, flow in the melt (MFI) of 6 g per 10 min and average molecular weight $189,000 \text{ g mol}^{-1}$); natural vermiculite from a Palabora deposit (South Africa) was supplied by Grena a.s., Czech Republic, with a particle size below $40 \mu\text{m}$ and cation exchange capacity (CEC) $89 \text{ cmol}(+)/\text{kg}$; natural graphite flakes (99%), supplied by Sigma Aldrich, Czech Republic, were used as the starting materials for the preparation of fillers and polymer nanocomposites. Graphene oxide was prepared from the graphite flakes using a modified Hummers' method. Vermiculite was modified in the first step using sodium chloride and in the second step using hexadecyl pyridinium bromide (HDP, >98%) or hexadecyltrimethylammonium bromide (HDTMA, >99%). Silver was anchored on vermiculite and graphene oxide surfaces using AgNO_3 (>98%). All chemicals, including those used for Hummers' method (i.e., potassium permanganate (KMnO_4), sulphuric acid (H_2SO_4), and hydrogen peroxide (H_2O_2)), were supplied by

Sigma-Aldrich, Prague, Czech Republic. Ultrapure MilliQ water (Merck) was used for all the aqueous solutions.

2.2. Methods of Preparation

2.2.1. Preparation of HDTMA and HDP-Modified Vermiculites (VMT + HDP and VMT + HDTMA)

The preparation of organically modified vermiculites was carried out following the procedure outlined in [37,39,40,56]. Natural vermiculite was saturated with Na⁺ cations to prepare the monoionic form of vermiculite (denoted as Na-VMT). Consequently, 100 g of Na-VMT was treated with aqueous solutions of HDP⁺ or HDTMA⁺ cations in quantities ensuring approximately 100% of cation exchange capacity ($1.0 \times \text{CEC}$). The prepared organovermiculites were washed repeatedly with demineralized water to remove halide ions (tested by AgNO₃ solution). Then, the samples were dried at 50 °C and stored in the dark at the laboratory temperature. The samples were denoted as VMT + HDP and VMT + HDTMA.

2.2.2. Preparation of VMT + Ag

Silver-modified vermiculite was prepared by intercalation of silver cations to the vermiculite structure from an aqueous solution, where 8.4 g of AgNO₃ was dissolved in 50 mL of demineralized water and 5 g of natural vermiculite was added to the solution. The suspension was shaken on a laboratory shaker for 24 h at the laboratory temperature and then heated to 70 °C for 3 h [36]. Finally, it was washed with demineralized water, dried at 50 °C, and stored in the dark at the laboratory temperature. The sample was denoted as VMT + AG.

2.2.3. Preparation GO and GO + Ag

Graphene oxide (GO) was prepared by a modified Hummers' method [55]. Briefly, 10 g of graphite was stirred with 250 mL of sulphuric acid (concentrated); then, 30 g of potassium permanganate was added, and the suspension was stirred for 3 h. Consequently, demineralized water was slowly added to the reaction mixture. Finally, 50 mL of hydrogen peroxide (30 wt.%) was added. The process was performed twice. The suspension was washed with demineralized water and dried at 50 °C and stored in dark.

For anchoring of Ag on the GO surface, 0.1 g of prepared GO was redissolved in demineralized water together with 11 g AgNO₃ in 100 mL of demineralized water. The suspension was stirred for 24 h at a laboratory temperature, then washed by demineralized water, dried at 50 °C, and stored in the dark at the laboratory temperature. The prepared sample was denoted as GO + Ag [38].

2.2.4. Preparation of Reinforced PLA Nanocomposite

Polymer nanocomposites were prepared by mixing 4 g of the granulated PLA with the individual fillers VMT + HDTMA, VMT + HDP, VMT + Ag, and GO + AG in a quantity of 1 wt.%. The mixture was homogenized using a Haake™ MiniLab polymer blender (ThermoFisher Scientific, Prague, Czech Republic) at 170 °C and 30 rpm for 5 min, then extruded in the shape of a string. The molecular weight of the PLA foils after the extrusion was checked by GPC; it was $184,500 \pm 700$ g/mol. The molecular weight of the original PLA pellets was 189,000 g/mol. The degradation reached approximately 2.4%; thus, it was from this point of view very low. It was confirmed also by XRD and FTIR analyses, the results of which were very similar. Strings of the polymer nanocomposite were pressed into a plate on a heat press at a temperature of 200 °C for 5 min; then, the formed plate was moved to a cold press until it cooled down. The prepared samples of reinforced PLA were denoted as PLA + VMT + HDTMA, PLA + VMT + HDP, PLA + VMT + AG, and PLA + GO + AG.

3. Methods of Characterizations

Several methods were used for the physicochemical characterization of prepared fillers and reinforced PLA. Efficient intercalation and anchoring processes were confirmed using the X-ray powder diffraction (XRD) method with an X-ray diffractometer Rigaku Ultima IV in the reflection mode, Bragg–Brentano arrangement, CuK α 1 radiation (RIGAKU Analytical devices, Inc., Wilmington, MA, USA) in the ambient atmosphere under constant conditions (40 kV, 40 mA). The content of Ag on the vermiculite and graphene oxide surfaces was confirmed using ICP-OES VISION EOP (SPECTRO Analytical Instruments GmbH, Kleve, Germany). The content of HDTMA⁺ and HDP⁺ cations in the inorganic vermiculite structure was determined by phase carbon analysis on the multi-phase carbon and water analyzer RC612 (LECO, St. Joseph, MI, USA).

The optical digital microscope, VHX-500 (Keyence International, Mechelen, Belgium), and a scanning electron microscope (SEM) were used for a surface morphology study of polymer composites. SEM was performed using samples sputter-coated with a thin film of gold by an electron microscope Quanta 450FEG (FEI, Hillsboro, OR, USA) with the following working conditions: accelerating voltage 10.0 kV, working distance 8.0 mm, and probe current 100 mA.

Thermogravimetric analysis (TGA) was conducted on a thermal analyzer STA 409EP (NETZSCH-Gerätebau GmbH, Selb, Germany) using an Al₂O₃ crucible in air and argon atmospheres with a heating rate of 10.0 K min^{−1} from 30 to 600 °C. The heat response of the nanocomposite samples was measured using a differential scanning calorimeter (DSC) DSC131 EVO (SETARAM Instrumentation, Caluire, France) in an Al crucible of 30 μ L. The samples were heated from −20 to 200 °C at a rate of 5 K min^{−1} in an argon atmosphere.

A CSM Micro-Hardness Tester using Vickers diamond indenter working with a nominal angle of 136° was used. For the tests, the micro-indentation parameters used approached speeds of 50 mm/min, contact loads of 20 mN, load rates of 2000 mN/min, unload rates of 2000 mN/min, maximum loads of 1000 mN, and 20 s of pause. In addition, this micro indentation test could be released in four steps: (1) Vickers indenter pecks the surface; (2) loading phase up until the maximum, and the maximum load used was 1000 mN; (3) holding the load, and it was completed to keep away from the creep influence on the unloading characteristics; (4) in the final step in the unloading phase [35,57].

The specific indication that we faced with the micro indentation test was the indentation depths, which are shown in Figure 1:

- h_t is the whole depth below a load, P_t ;
- h_e is the elastic rebound depth for the unloading duration;
- h_f is the depth of the residual impression;
- h_a is the surface displacement at the perimeter;
- h_p is the depth of the contact indentation.

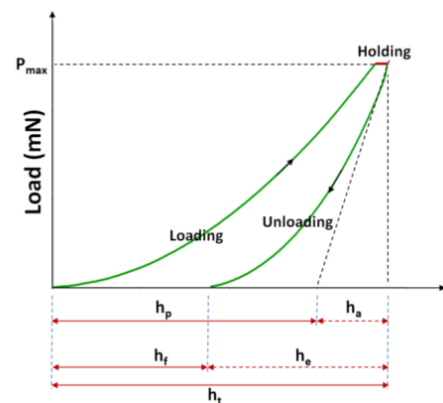
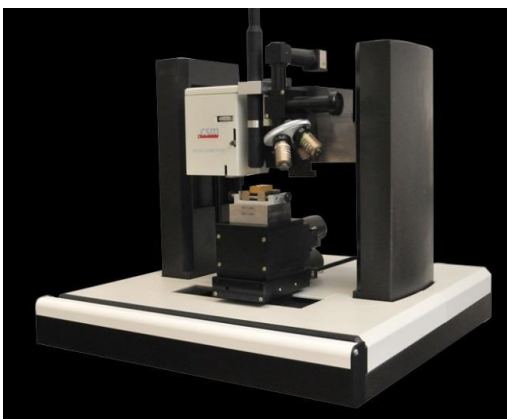


Figure 1. Indentation machine and representative plot of the load versus displacement.

The hardness, VHN, in this work is well defined as the test force divided by the indentation apparent area at maximal force:

$$\text{VHN} = \frac{P}{A}$$

where P is the maximum load, and A is the deep-sensing instrument.

The apparent elastic modulus was calculated from the following equation:

$$E = \frac{1 - \nu_s^P}{\frac{1}{E_r} - \frac{1 - \nu_i^2}{E_i}}$$

where E_i is the diamond indenter elastic modulus (1141 GPa), ν_i is the Poisson's ratio of the diamond indenter (0.07), E_r is the reduced modulus of the indentation contact, and ν_s is the Poisson's ratio of the bone (0.3).

4. Results and Discussion

4.1. Fillers Characterization by X-ray Diffraction

XRD analyses confirmed the presence of silver atoms on graphene oxide and vermiculite surfaces as well as the presence of HDTMA⁺ and HDP⁺ in the vermiculite structure. Data are not presented here.

The quantity of Ag anchored on graphene oxide and vermiculite matrices was determined to be 61 ± 10 wt.% and 8.94 ± 1.35 wt.%, respectively. The difference in the Ag content on GO and vermiculite surfaces was conducted by a different method of modification, but it was corresponding as one can see: in the case of GO, a higher quantity of Ag⁺ was used, while for GO + Ag the Ag⁺/GO ratio was 6.35 and for VMT + AG it was 1.07.

The number of the organic cations, HDTMA⁺ and HDP⁺, in the VMT matrices was confirmed by the phase carbon analysis. The organic carbon content in the vermiculite structure was determined to be 24.5 and 20.2 wt.%, respectively. It proved that the intercalation was successful; the cation exchange was 120 and 90%, respectively, which corresponds with our previous findings in Plachá (2008, 2010) [39,56].

4.2. Morphological and Structural Characteristics of Reinforced PLA Nanocomposite

Reinforced PLA samples were characterized using the optical digital microscope (KEYENCE) and a scanning electron microscope (SEM) to describe surface morphology. In Figure 2, the individual polymer nanocomposites together with the pure PLA polymer are presented. There was a clear difference comparing the pure PLA and the PLA containing various fillers. The surface of reinforced PLA samples seemed to be smooth and the fillers were distributed in the whole area. The particle size of fillers was not uniform, and the composites contained both nano- and microparticles.

Figure 3 represents SEM images of the pure PLA and reinforced PLA samples. While the pure PLA had a smooth surface without any particles, the composites contained particles that rose to the surface of the composites. The least uniform particles were contained in the PLA + GO + Ag, and the PLA filled with organically modified vermiculites seemed to be the most homogenous.

4.3. Thermal Stability by Thermogravimetric Analysis

Thermogravimetric analysis of polymer composites together with the sample of the pure PLA was performed in air and argon atmospheres. No information on the composition of the technical PLA was given by the vendor. The TGA showed the thermal stability of the prepared composites under rising temperatures. The results are presented in Figure 4. It was observed that the pure PLA followed the one-step degradation between 330.4 and 368.2 °C in the air atmosphere (Figure 5) and 336.1 and 374.4 °C (Figure 4b) in the argon atmosphere, which corresponds with observations reported elsewhere.

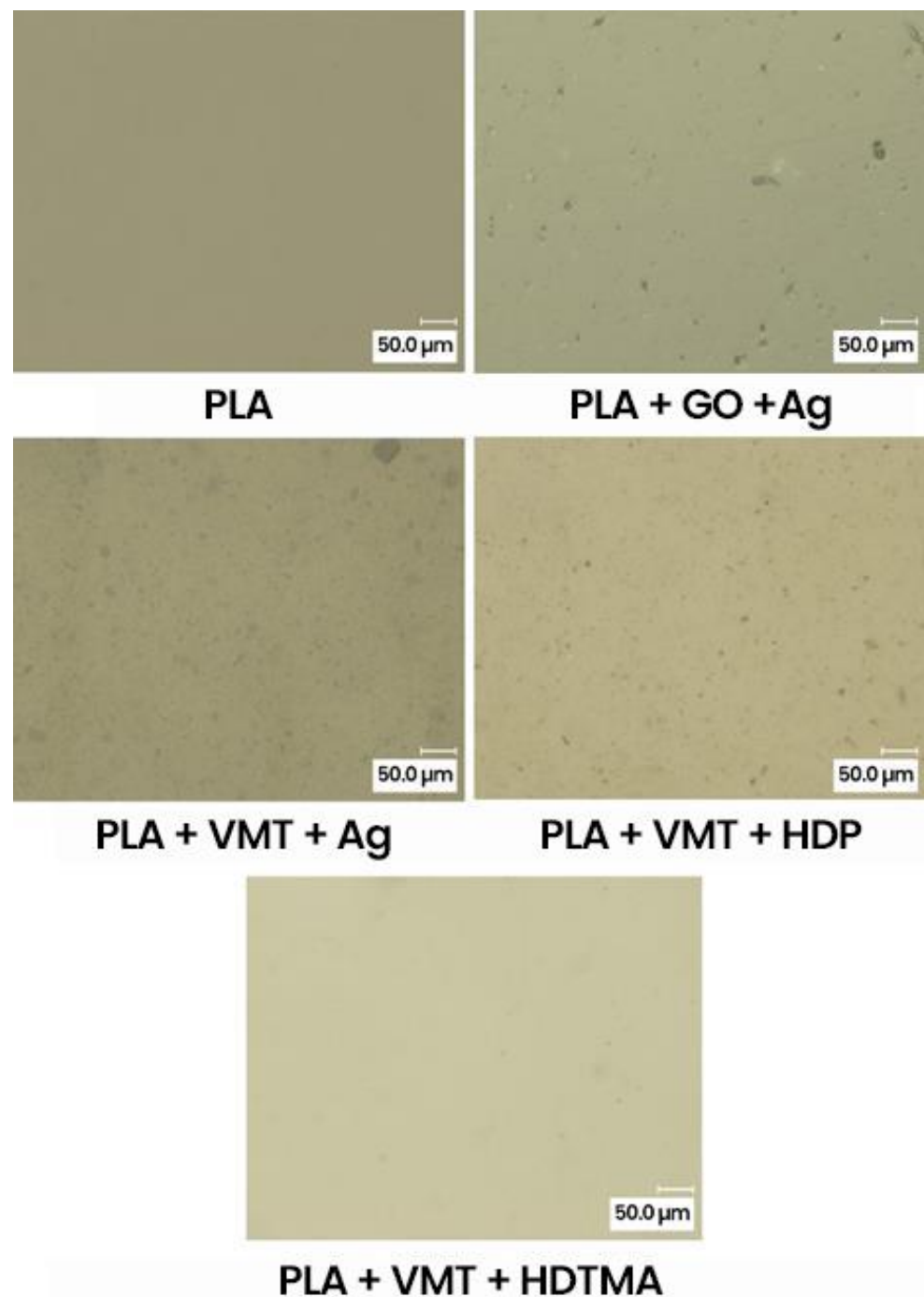


Figure 2. Optical microscopy (KEYENCE) of the different polymer composites.

Thermal degradation of the reinforced PLA samples in the air atmosphere (Figure 4a) was shifted to lower temperature values, except for PLA + GO + Ag, where the initial degradation temperature (329.9 °C) was almost identical to the start of degradation for the pure PLA, and the end of degradation was set at a higher temperature of 370.9 °C. Reinforcement of PLA using GO + Ag did not impair the thermal stability of PLA. In the case of PLA with modified-vermiculite loadings, the degradation temperature ranges shifted to lower temperatures: 327.2–364.7, 328.7–367.4, and 328.3–366.2 °C for PLA + VMT + Ag, PLA + VMT + HDTMA, and PLA + VMT + HDP, respectively (Figure 4a). In the argon atmosphere (Figure 4b), the temperature degradation proceeded faster, and the temperature interval narrowed compared to the pure PLA. The temperature range was 335.2–369.9,

337.3–368.6, 324.1–361.4, and 327.9–364.6 °C for PLA + GO + Ag, PLA + VMT + Ag, PLA + VMT + HDTMA, and PLA + VMT + HDP, respectively. In all cases, the thermal degradation started earlier than in the pure PLA except for PLA + VMT + Ag, and the final temperature was shifted in all cases to the lower temperatures by 6 °C or more. The composites PLA + VMT + HDTMA and PLA + VMT + HDP showed the worst thermal stability in the inert atmosphere.

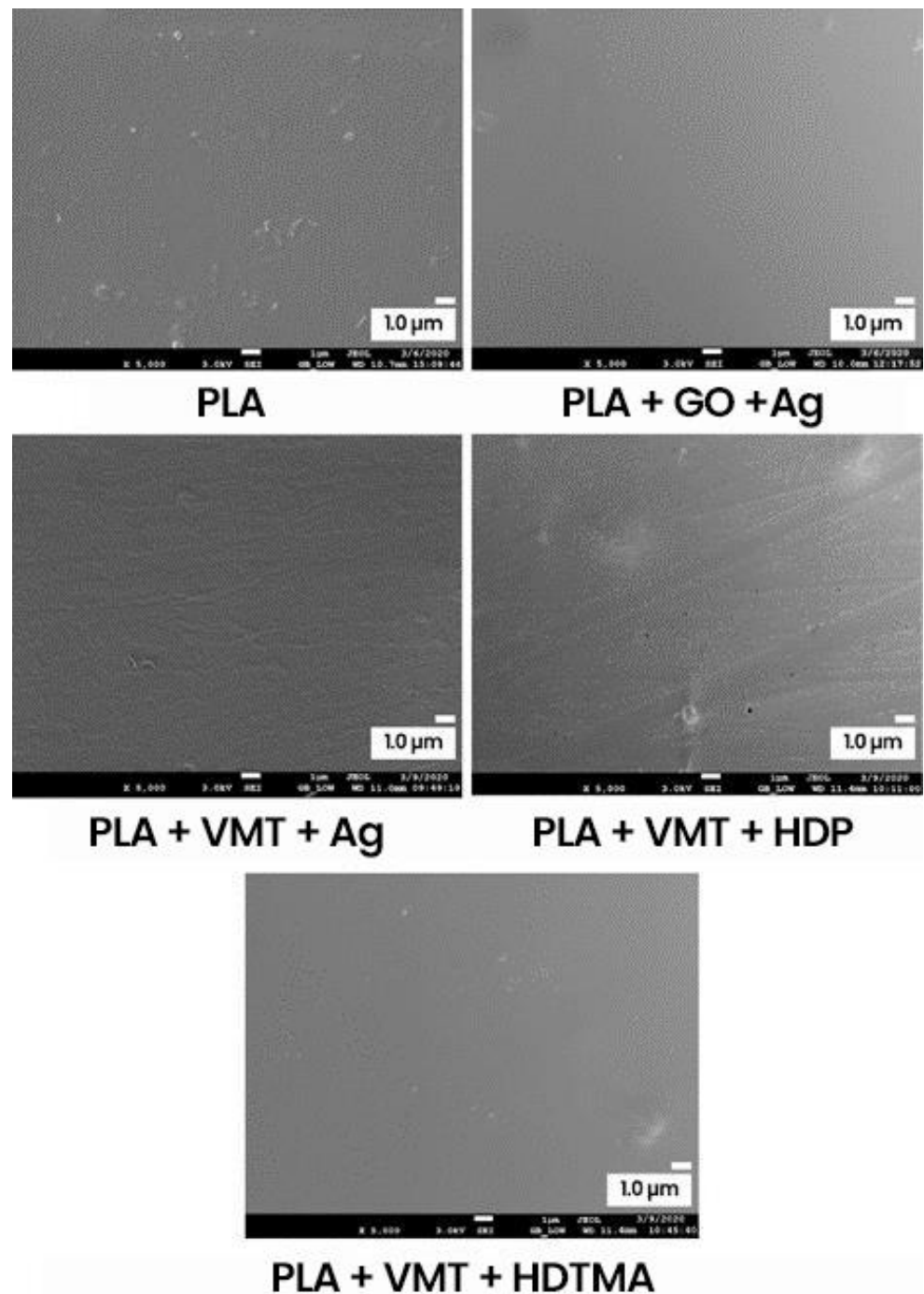


Figure 3. SEM images of different polymer composites.

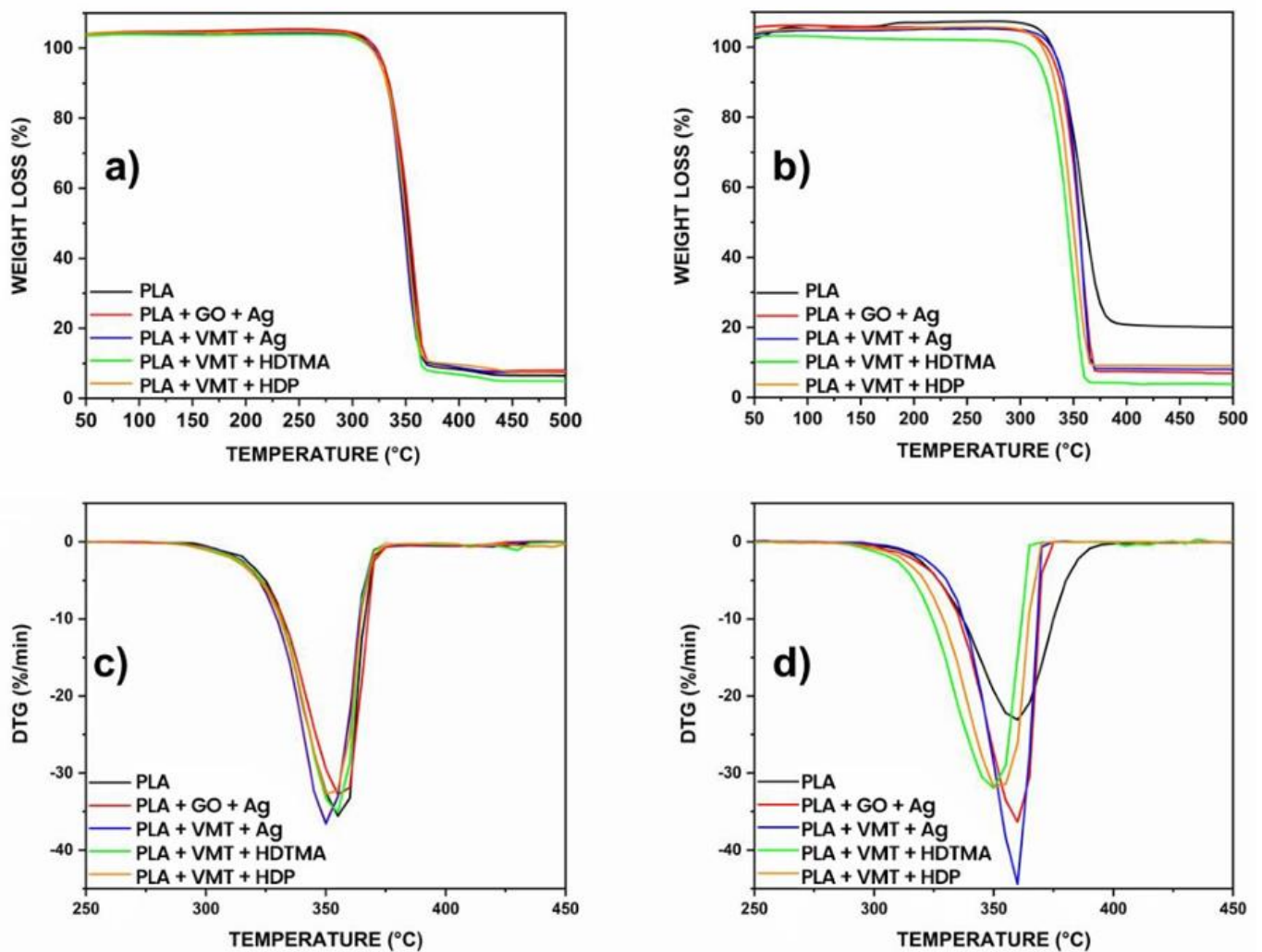


Figure 4. TGA curves of the pure PLA and reinforced PLA specimens (a) in the air atmosphere; (b) in the inert atmosphere. DTG curves of the pure PLA and the reinforced PLA specimens (c) in the air atmosphere; (d) in the inert atmosphere.

The effect of reinforcement on thermal stability was precisely analyzed using first derivative (DTG) curves (Figure 4c,d). The peak at a particular temperature shows the degradation temperature of the polymer specimens. It was confirmed that in the air atmosphere (Figure 4c), GO + Ag filler increased the thermal stability of the pure PLA by 2.3 °C, and the VMT + HDTMA and VMT + HDP fillers were comparable even if they had lower thermal stability than the pure PLA. The filler VMT + Ag showed the worst thermal stability of the composite. In the inert atmosphere (Figure 4d), all reinforcements showed lower thermal stability than the pure PLA, the reinforcements containing Ag by approximately 6 °C, in the case of the organically modified vermiculites by 12.7 and 8.9 °C for VMT + HDTMA and VMT + HDP.

4.4. Thermal Properties by DSC

Table 1 summarizes the observed DSC results of the pure and reinforced PLA, namely, the glass transition temperature (T_g), cold crystallization temperature (T_c), and melts temperature (T_m). Representative DSC curves are shown in Figure 5. We can observe a slight variation in the PLA and the reinforced PLA curves around 60–61 °C relative to the T_g of PLA. The T_g of PLA practically did not change in the presence of reinforcements; it very slightly decreased. A cold crystallization peak (T_c) for PLA was at 105.85 °C. There was a gentle drop of the T_c for PLA + VMT + HDTMA and PLA + VMT + HDP to 104.67

and 105.23 °C, respectively. However, in PLA + GO + Ag and PLA + VMT + Ag, the T_c value shifted to higher values of 122.54 and 109.76 °C.

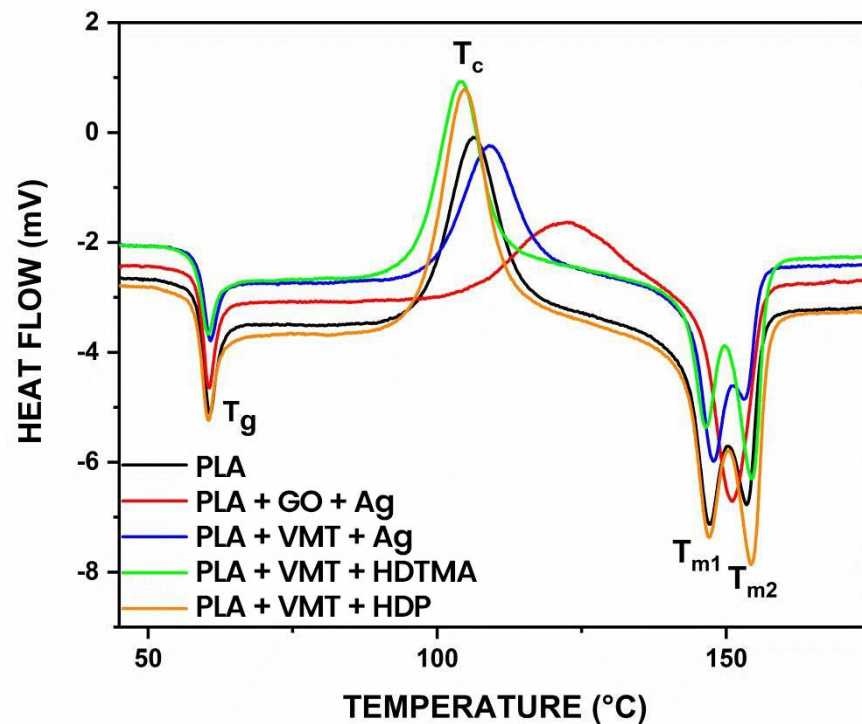


Figure 5. DSC curves of the pure and reinforced PLA.

Table 1. DSC results of the pure PLA and reinforced PLA specimens.

Temperature (°C)	PLA	PLA + GO + Ag	PLA + VMT + Ag	PLA + VMT + HDTMA	PLA + VMT + HDP
T_g	60.86	60.71	60.77	60.34	60.18
T_c	105.85	122.54	109.76	104.67	105.23
T_{m1}	147.15	-	147.90	146.72	147.42
T_{m2}	153.62	151.07	153.52	154.52	154.92

Two peaks, T_{m1} and T_{m2} , for the melting temperature of PLA occurred at 147.15 and 153.62 °C, respectively. The double peak in the PLA curve can be explained by the fact that the heating rate was so low that smaller PLA crystals could melt and recrystallize. Addition or reinforcements to the PLA did not influence the melting temperature values, except for GO + Ag. In that case, only one melting temperature peak was observed at 151.07 °C, influenced by the formation of a disordered alpha phase and the existence of more than one crystalline structure.

4.5. Mechanical Response

Microhardness measurements were accomplished to preliminarily evaluate the mechanical response displayed by these materials after their treatment. The load-displacement curves for the neat PLA and each reinforced PLA are presented in Figure 6. These curves contribute to evaluating the elastic to plastic behavior of the samples at the surface. Figure 6 presents the P- δ interactions of different charges, such as VMT + Ag, GO + Ag, VMT + HDP, and VMT + HDTMA additives specimens, which were obtained using an indentation apparatus.

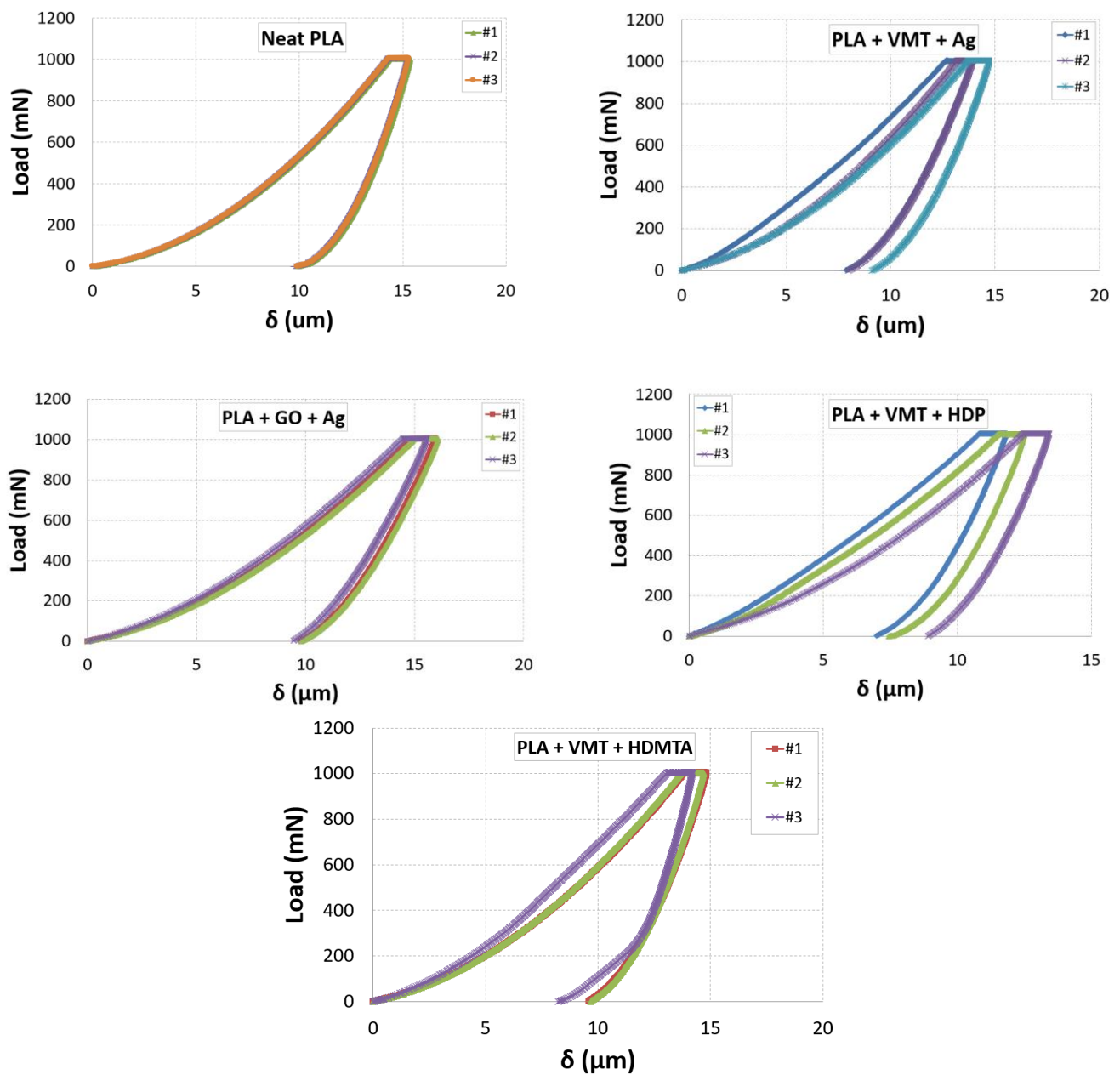


Figure 6. Indentation profiles for the different materials.

According to the neat PLA, as shown in Figure 7, the reinforced PLA sample displayed a significantly higher indentation load (P) for some of the types of charges, e.g., the value of P roughly increased by 28.07%, 31.44%, 49.70%, and 60.70% with the addition of VMT + Ag, GO + Ag, VMT + HDTMA, and VMT + HDP, correspondingly, at $\delta = 5 \mu\text{m}$. This means that the reinforcement particles created a significant contribution to the whole reinforced PLA indentation response. The same inspection can be created for the indenter displacement.

Certainly, as shown in Figure 8, with the addition of the VMT + HDP and VMT + HDTMA particles, there was an increase in stiffness and, consequently, a decrease in the displacement at a force of 1000 mN. In comparison to neat PLA, the displacement decreased by 1.04%, 4.22%, 7.54%, and 12.68% with the addition of GO + Ag, VMT + Ag, VMT + HDTMA, and VMT + HDP, respectively (Figure 6). In this case, we can prove that these additives contributed to obtaining a good toughness for the PLA matrix. For both PLA and reinforced PLA specimens, the indentation deformation was not able to improve after unloading, which implies that their deformations were not elastic; there is dissimilarity concerning the

loading curves and unloading. In this figure, it is possible to detect that as the type of the additive changed, the rigidity of the material also changed.

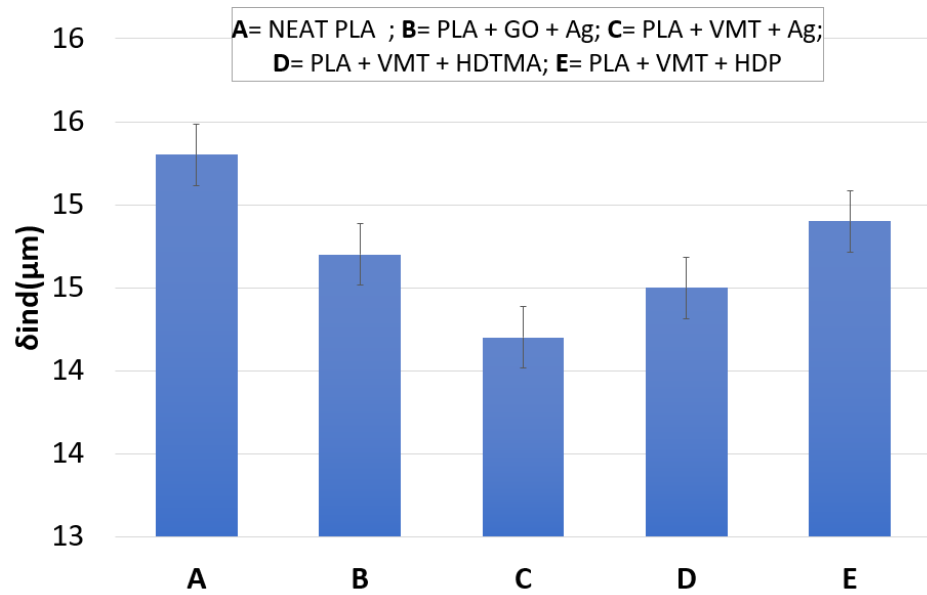


Figure 7. Effect of the additives on the displacement of the reinforced PLA.

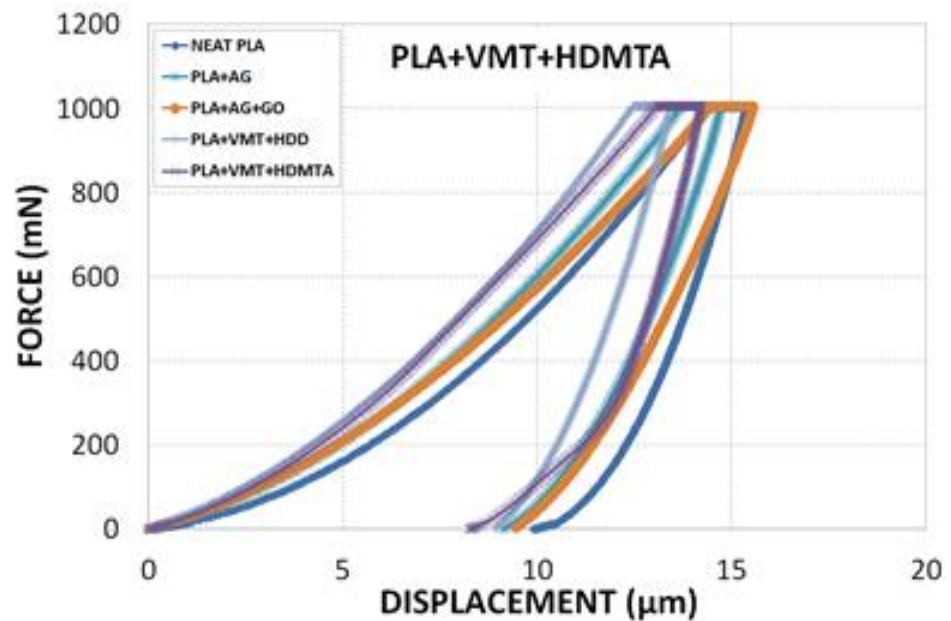


Figure 8. Effect of additives on the local mechanical behavior using indentation tests.

Figure 9 shows the considered apparent elastic modulus depending on the additive of reinforcement. The addition of VMT + HDTMA and VMT + HDP into the PLA matrix presented improved resistance of the interfacial, thus increasing the apparent elastic modulus from 5.372 to 6.620 GPa. This enhancement is owed to the high aspect ratio and intrinsic mechanical performance of VMT + HDP and VMT + HDTMA in comparison to the PLA matrix. However, adding VMT + Ag and GO + AG into the PLA matrix decreased the mechanical performance, thereby decreasing the apparent elastic modulus from 5.372 to 3.820 GPa.

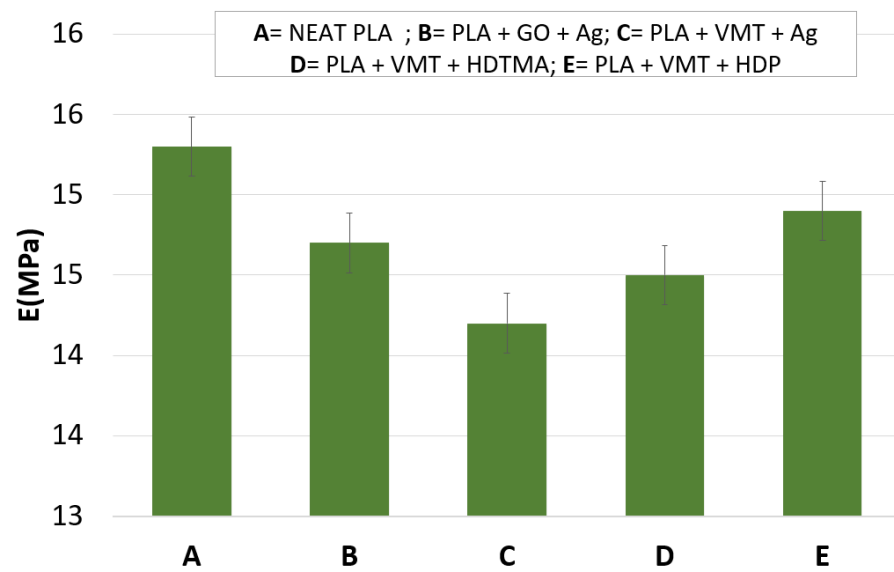


Figure 9. Effect of additives on the apparent elastic modulus.

In this work, PLA + VMT + HDP exhibited a high apparent elastic modulus, demonstrating its superior structural performance compared to neat PLA and other present reinforced PLA. As previously stated, the apparent elastic modulus increased with increasing filler loading, because the fillers absorb the stress transferred from the PLA matrix. In other words, as the concentration of reinforced PLA polymer increased, so did the chain entanglements and solution viscosity which, in turn, increased the viscoelastic force.

Figure 10 demonstrates that the reinforced PLA matrices with the VMT + HDTMA and VMT + HDP additives had much better resistance to indentation than the individual neat PLA stiffness. However, the addition of GO + Ag and VMT + Ag additives contributed to degrading the material performance of the PLA. It made the material less stiff and affected the material's life and fragility in front of the fatigue; it cannot be resistant for a long time.

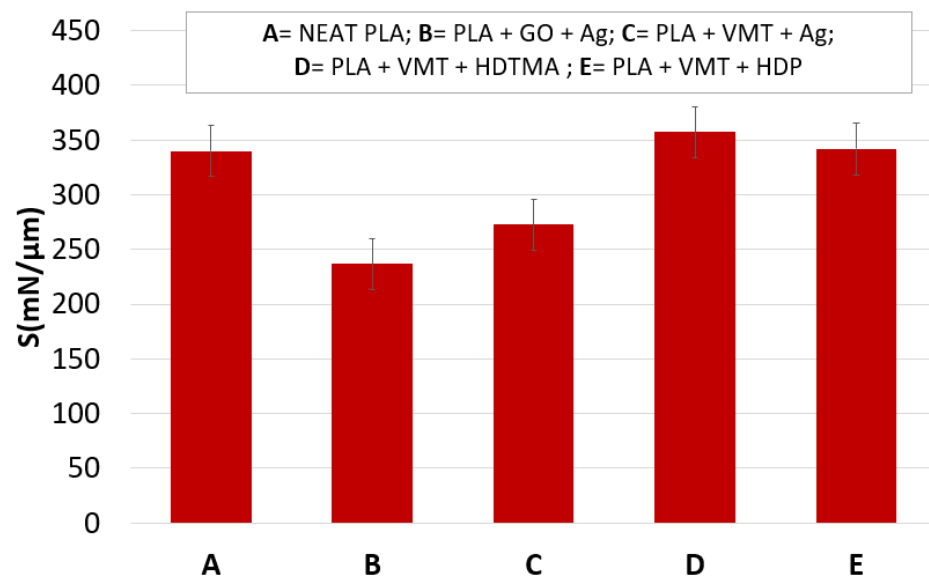


Figure 10. Effect of additive type on stiffness.

Figure 11 confirms the effect of a different kind of charge content on the hardness of the reinforced PLA. An enhancement in the hardness was detected with the addition of VMT + Ag, GO + Ag, VMT + HDP, and VMT + HDTMA. The neat PLA samples exhibited a hardness of 25.196 Vickers, which increased to 38.855 (54.212%), 38.581 (34.69%), 53.123

(56.77%), and 54.953 (118.102%) with the addition of VMT + Ag, GO + Ag, VMT + HDTMA, and VMT + HDP, correspondingly. This increase in hardness was due to the reliable distribution and interfacial bonding concerning nanoadditives and the PLA matrix (Table 2).

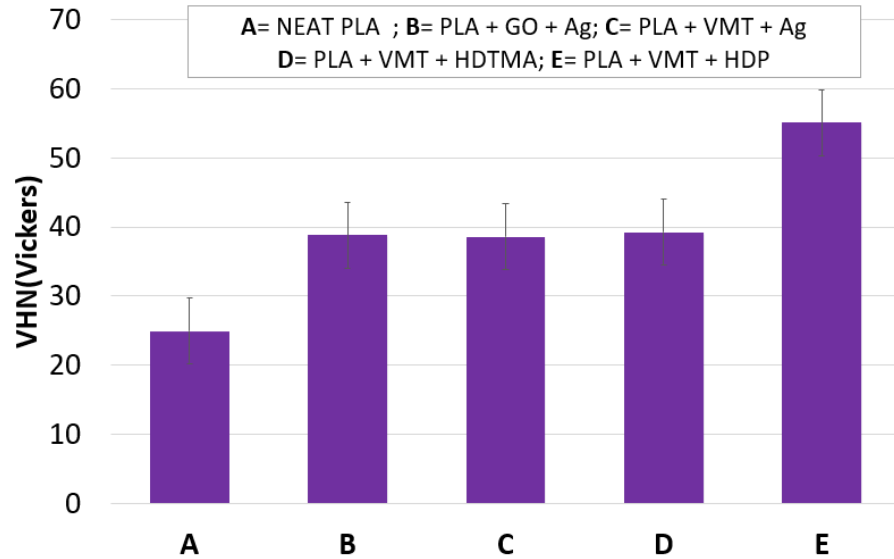


Figure 11. Effect of additives type on the reinforced PLA’s hardness.

Table 2. Representative table of the averAge and error barres of each plaque.

		Neat PLA	PLA VMT + Ag	PLA GO + Ag	PLA VMT + HDTMA	PLA VMT + VDP
E (GPa)	AverAge	5.372	4.972	3.820	5.833	6.620
	SD	0.161	0.286	0.0553	1.100	0.366
Hv (Vickers)	AverAge	25.196	38.855	38.581	39.501	54.953
	SD	18.349	3.987	1.891	0.526	7.452
S (mN/μm)	AverAge	337.569	271.123	233.747	356.687	343.598
	SD	3.099	15.004	11.450	69.461	4.554
D (μm)	AverAge	15.330	14.300	14.810	14.580	12.960
	SD	0.0566	0.594	0.584	0.329	0.650

The Print Effects

The value of the Vickers HV hardness is given by the ratio of the load applied to the projected area of the residual impression. It is deduced from the dimensions of the diAgonals of the residual imprint produced on the surface of the material according to Equation (1).

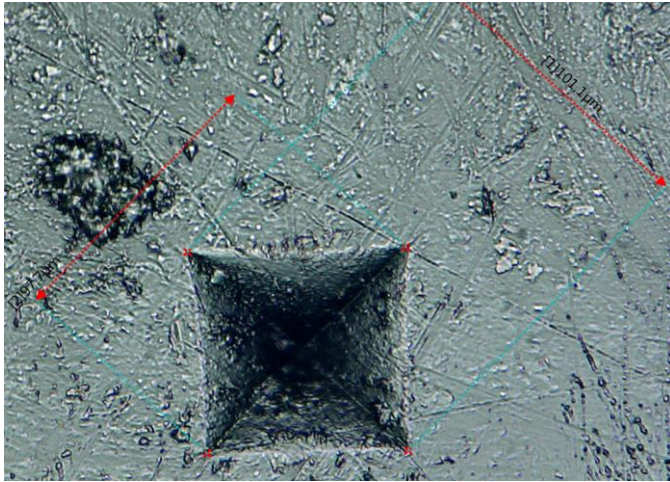
$$1 \times 10^3 \times \frac{P}{A_s} = 2 \times 10^3 \frac{P \cdot \sin(\frac{\alpha}{2})}{d_v^2} = 0.0018544 \times \frac{P}{d_v^2} \tag{1}$$

where P is the load applied in N, A_s is the actual surface area of the cavity in mm², d_v is the averAge of the diAgonal lengths d₁ and d₂ of the cavity in mm, α is the angle between the faces of the indenter (136°), and HV is in GPa.

Here, one can mention that surface area has a significant effect on the hardness of materials. In Figure 12 and depending on the variation of the surface area of the print with each material, one can mention it can give an impression of the kind of reaction material and its resistance. In our example, it is remarkable that the big surface area of the footprint was only with the PLA reinforced with VMT + Ag which explains its brittle reaction of surface material. However, the smallest area was observed with PLA reinforced with VMT + HDTMA which explains their good performance and resistance to impact imposed

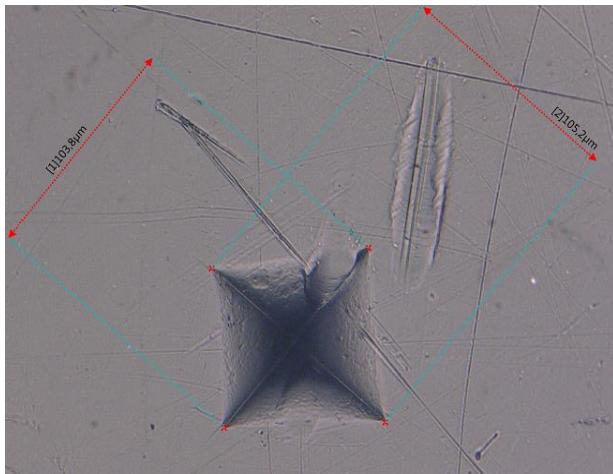
from the indenter, which is why we can prove that the print gives us an impression on the hardness of the surface from one surface area to another.

PLA + VMT + Ag



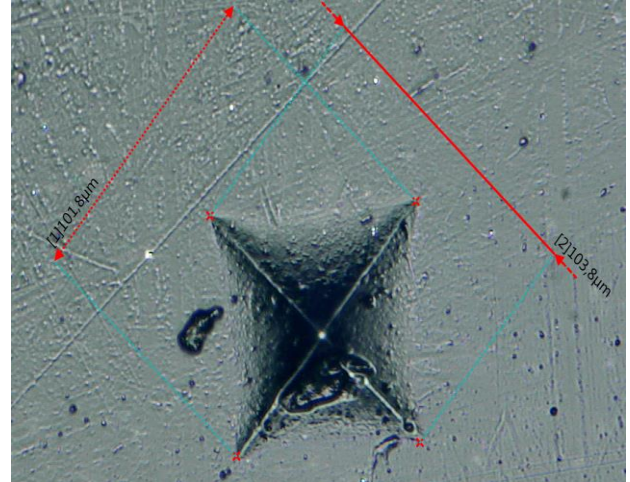
$$dm = 99.4 \text{ Ar} = 1.876 \cdot 10^{-13} \mu\text{m}^2$$

PLA + VMT + HDP



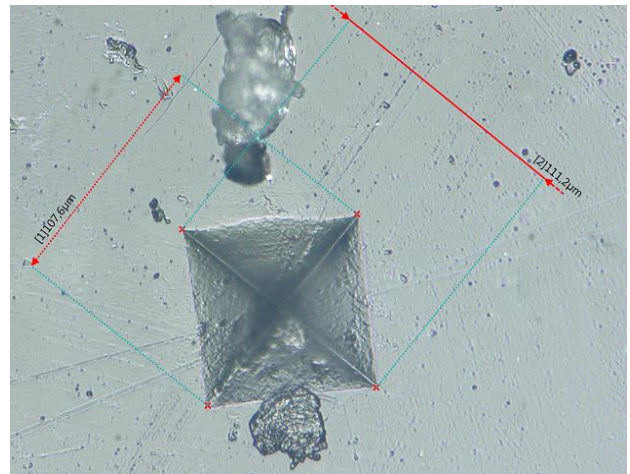
$$dm = 103.5 \text{ Ar} = 1.73 \cdot 10^{-13} \mu\text{m}^2$$

PLA + GO + Ag



$$dm = 102.8 \text{ Ar} = 1.754 \cdot 10^{-13} \mu\text{m}^2$$

PLA + VMT + HDTMA



$$dm = 109.4 \text{ Ar} = 1.54 \cdot 10^{-13} \mu\text{m}^2$$

Figure 12. Effect of the hardness of the samples on the print surface area.

5. Conclusions

In this study, unreinforced and reinforced PLA nanocomposites were investigated. Their morphology, changes in the PLA phase and its transformation, and some final properties, such as thermal stability and mechanical behavior, were systematically investigated.

The Tg of PLA did not change with the reinforcement, it only decreased very slightly. However, for PLA + GO + Ag and PLA + VMT + Ag, the Tc values shifted to higher values of 122.54 and 109.76 °C. In an air atmosphere, the GO + Ag filler improved the thermal stability of pure PLA by 2.3 °C, while the VMT + HDTMA and VMT + HDP fillers exhibited comparable, albeit lower, thermal stability. The filler VMT + GO + Ag composite had the lowest thermal stability.

In an inert atmosphere, the thermal stability of all reinforcements was lower than that of pure PLA for VMT + HDTMA and VMT + HDP, approximately 6 °C for AG reinforcement and 12.7 and 8.9 °C for organically modified vermiculite, respectively. Furthermore, it

was established that including VMT + HDTMA in a PLA matrix reduced the depth of indentation (d) and increased the apparent elastic modulus (E), stiffness (S), and hardness (H). The results of this report indicate that the reinforced PLA with VMT + HDTMA has higher potential as a structural material

In this work, we concluded that the fillers used to reinforce the PLA's performance are similar from the point of view of physicochemical properties, but in terms of mechanical properties, they present an evident difference.

Ultimately, these polymeric nanocomposites could be used for biomedical applications such as temporary body implants (fracture fixation screws, stents, absorbable sutures, bandAges, etc.) or antimicrobial surgical devices (catheters and others).

For that reason, the following intention for the use of prepared nanocomposites is to test their antimicrobial properties, which will be manifested in a longer time horizon to prevent long-term biofilm formation and also to test their ability to be material for 3D printing.

Author Contributions: S.K.: Investigation, Methodology, Writing—original draft; M.T.: Methodology, Investigation, Project administration, Conceptualization, Writing—original draft, Writing review & editing, Funding acquisition; D.P.: Methodology, Investigation, Writing—original draft, Project administration, Writing—review & editing; K.Š., D.M. and F.E.: Validation, Visualization. All authors have read and agreed to the published version of the manuscript.

Funding: This work was kindly supported by the Ministry of Education of the Czech Republic through the SGS projects: SP2019/23 “Development of Biocompatible Nanocomposite Materials with Antimicrobial Effects” and SP2020/70 “New Functional Fillers for Nanocomposite Materials”. This work is part of a collaboration between ENSTA Bretagne and the Technical University of Ostrava in the framework of Campus France funding (Barrande 2020). [M42] [SK3].

Institutional Review Board Statement: Not applicable.

Informed Consent Statement: Not applicable.

Data Availability Statement: Not applicable.

Acknowledgments: The authors thank very much Silvia Vallová and Lucie Chlebíková (Technical University of Ostrava) for performing the TGA and DSC analyses.

Conflicts of Interest: The authors declare no conflict of interest.

References

1. Cheng, Y.; Deng, S.; Chen, P.; Ruan, R. Polylactic acid (PLA) synthesis and modifications: A review. *Front. Chem. China* **2009**, *4*, 259–264. [[CrossRef](#)]
2. Garlotta, D. A Literature Review of Poly(Lactic Acid). *J. Polym. Environ.* **2001**, *9*, 63–84. [[CrossRef](#)]
3. Sharif, A.; Mondal, S.; Hoque, M.E. Polylactic acid (PLA)-based nanocomposites: Processing and properties. In *Bio-Based Polymers and Nanocomposites*; Springer: Cham, Switzerland, 2019; pp. 233–254.
4. Bhardwaj, R.; Mohanty, A.K. Modification of Brittle Polylactide by Novel Hyperbranched Polymer-Based Nanostructures. *Biomacromolecules* **2007**, *8*, 2476–2484. [[CrossRef](#)] [[PubMed](#)]
5. Kim, S.; Hyon, S.; Kim, C. Distributed virtual negative-sequence impedance control for accurate imbalance power sharing in islanded microgrids. *Sustain. Energy Grids Netw.* **2018**, *16*, 28–36. [[CrossRef](#)]
6. Heidari, B.S.; Oliaei, E.; Shayesteh, H.; Davachi, S.M.; Hejazi, I.; Seyfi, J.; Bahrami, M.; Rashedi, H. Simulation of mechanical behavior and optimization of simulated injection molding process for PLA based antibacterial composite and nanocomposite bone screws using central composite design. *J. Mech. Behav. Biomed. Mater.* **2017**, *65*, 160–176. [[CrossRef](#)]
7. Zare, Y.; Rhee, K.Y. Expression of normal stress difference and relaxation modulus for ternary nanocomposites containing biodegradable polymers and carbon nanotubes by storAge and loss modulus data. *Compos. Part B Eng.* **2019**, *158*, 162–168. [[CrossRef](#)]
8. Škrlová, K.; Malachová, K.; Muñoz-Bonilla, A.; Měřinská, D.; Rybková, Z.; Fernández-García, M.; Plachá, D. Biocompatible polymer materials with antimicrobial properties for preparation of stents. *Nanomaterials* **2019**, *9*, 1548. [[CrossRef](#)]
9. JAgadish, R.S.; Raj, B.; Asha, M.R. Blending of low-density polyethylene with vanillin for improved barrier and aroma-releasing properties in food packAging. *J. Appl. Polym. Sci.* **2009**, *113*, 3732–3741. [[CrossRef](#)]
10. Luo, Y.-B.; Wang, X.-L.; Wang, Y.-Z. Effect of TiO₂ nanoparticles on the long-term hydrolytic degradation behavior of PLA. *Polym. Degrad. Stab.* **2012**, *97*, 721–728. [[CrossRef](#)]

11. Fukushima, K.; Tabuani, D.; Abbate, C.; Arena, M.; Ferreri, L. Effect of sepiolite on the biodegradation of poly (lactic acid) and polycaprolactone. *Polym. Degrad. Stab.* **2010**, *95*, 2049–2056. [[CrossRef](#)]
12. Fukushima, K.; Abbate, C.; Tabuani, D.; Gennari, M.; Camino, G. Biodegradation of poly (lactic acid) and its nanocomposites. *Polym. Degrad. Stab.* **2009**, *94*, 1646–1655. [[CrossRef](#)]
13. Pyda, M.; Wunderlich, B. Reversing and nonreversing heat capacity of poly (lactic acid) in the glass transition region by TMDSC. *Macromolecules* **2005**, *38*, 10472–10479. [[CrossRef](#)]
14. Södergård, A.; Stolt, M. Properties of lactic acid based polymers and their correlation with composition. *Prog. Polym. Sci.* **2002**, *27*, 1123–1163. [[CrossRef](#)]
15. Barczewski, M.; Mysiukiewicz, O.; Hejna, A.; Biskup, R.; Szulc, J.; Michałowski, S.; Piasecki, A.; Kloziński, A. The Effect of Surface Treatment with Isocyanate and Aromatic Carbodiimide of Thermally Expanded Vermiculite Used as a Functional Filler for Polylactide-Based Composites. *Polymers* **2021**, *13*, 890. [[CrossRef](#)]
16. Bordes, P.; Pollet, E.; Avérous, L. Nano-biocomposites: Biodegradable polyester/nanoclay systems. *Prog. Polym. Sci.* **2009**, *34*, 125–155. [[CrossRef](#)]
17. Bledzki, A.K.; Franciszczak, P.; Meljon, A. High performance hybrid PP and PLA biocomposites reinforced with short man-made cellulose fibres and softwood flour. *Compos. Part A Appl. Sci. Manuf.* **2015**, *74*, 132–139. [[CrossRef](#)]
18. Fortunati, E.; Peltzer, M.; Armentano, I.; Jiménez, A.; Kenny, J.M. Combined effects of cellulose nanocrystals and silver nanoparticles on the barrier and migration properties of PLA nano-biocomposites. *J. Food Eng.* **2013**, *118*, 117–124. [[CrossRef](#)]
19. Martino, V.P.; Jimenez, A.; Ruseckaite, R.A.; Averous, L. Structure and properties of clay nano-biocomposites based on poly (lactic acid) plasticized with polyadipates. *Polym. Adv. Technol.* **2011**, *22*, 2206–2213. [[CrossRef](#)]
20. Hossain, K.M.Z.; Ahmed, I.; Parsons, A.J.; Scotchford, C.A.; Walker, G.S.; Thielemans, W.; Rudd, C.D. Physico-chemical and mechanical properties of nanocomposites prepared using cellulose nanowhiskers and poly(lactic acid). *J. Mater. Sci.* **2012**, *47*, 2675–2686. [[CrossRef](#)]
21. Ramos, M.; Fortunati, E.; Peltzer, M.; Dominici, F.; Jiménez, A.; del Carmen Garrigós, M.; Kenny, J.M. Influence of thymol and silver nanoparticles on the degradation of poly(lactic acid) based nanocomposites: Thermal and morphological properties. *Polym. Degrad. Stab.* **2014**, *108*, 158–165. [[CrossRef](#)]
22. Andrzejewski, J.; Cheng, J.; Anstey, A.; Mohanty, A.K.; Misra, M. Development of Toughened Blends of Poly(lactic acid) and Poly(butylene adipate-co-terephthalate) for 3D Printing Applications: Compatibilization Methods and Material Performance Evaluation. *ACS Sustain. Chem. Eng.* **2020**, *8*, 6576–6589. [[CrossRef](#)]
23. Murariu, M.; Dubois, P. PLA composites: From production to properties. *Adv. Drug Deliv. Rev.* **2016**, *107*, 17–46. [[CrossRef](#)] [[PubMed](#)]
24. Piekarska, K.; Piorkowska, E.; Bojda, J. The influence of matrix crystallinity, filler grain size and modification on properties of PLA/calcium carbonate composites. *Polym. Test.* **2017**, *62*, 203–209. [[CrossRef](#)]
25. Wen, B.; Ma, L.; Zou, W.; Zheng, X. Enhanced thermal conductivity of poly(lactic acid)/alumina composite by synergistic effect of tuning crystallization of poly(lactic acid) crystallization and filler content. *J. Mater. Sci. Mater. Electron.* **2020**, *31*, 6328–6338. [[CrossRef](#)]
26. Tenn, N.; Follain, N.; Soulestin, J.; Crétois, R.; Bourbigot, S.; Marais, S. Effect of Nanoclay Hydration on Barrier Properties of PLA/Montmorillonite Based Nanocomposites. *J. Phys. Chem. C* **2013**, *117*, 12117–12135. [[CrossRef](#)]
27. Alves, J.L.; de Tarso Vieira e Rosa, P.; Realinho, V.; Antunes, M.; Velasco, J.I.; Morales, A.R. The effect of Brazilian organic-modified montmorillonites on the thermal stability and fire performance of organoclay-filled PLA nanocomposites. *Appl. Clay Sci.* **2020**, *194*, 105697. [[CrossRef](#)]
28. Wang, G.; Zhang, D.; Wan, G.; Li, B.; Zhao, G. Glass fiber reinforced PLA composite with enhanced mechanical properties, thermal behavior, and foaming ability. *Polymer* **2019**, *181*, 121803. [[CrossRef](#)]
29. Pan, H.; Kong, J.; Chen, Y.; Zhang, H.; Dong, L. Improved heat resistance properties of poly(l-lactide)/basalt fiber biocomposites with high crystallinity under forming hybrid-crystalline morphology. *Int. J. Biol. Macromol.* **2019**, *122*, 848–856. [[CrossRef](#)]
30. Wu, D.; Wu, L.; Sun, Y.; Zhang, M. Rheological properties and crystallization behavior of multi-walled carbon nanotube/poly (ϵ -caprolactone) composites. *J. Polym. Sci. Part B Polym. Phys.* **2007**, *45*, 3137–3147. [[CrossRef](#)]
31. Cacopardo, L.; Guazzelli, N.; Ahluwalia, A. Characterizing and Engineering Biomimetic Materials for Viscoelastic Mechanotransduction Studies. *Tissue Eng. Part B Rev.* **2021**, *ahead of print*. [[CrossRef](#)]
32. Khammassi, S.; Tarfaoui, M.; Lafdi, K. Study of mechanical performance of polymer nanocomposites reinforced with exfoliated graphite of different mesh sizes using micro-indentation. *J. Compos. Mater.* **2021**, *55*, 2617–2629. [[CrossRef](#)]
33. Khammassi, S.; Tarfaoui, M. Micromechanical characterization of Carbon Black reinforced adhesive nanocomposite using micro indentation. *Mater. Today Proc.* **2021**, *52*, 222–226. [[CrossRef](#)]
34. Khammassi, S.; Tarfaoui, M. Influence of exfoliated graphite filler size on the electrical, thermal, and mechanical polymer properties. *J. Compos. Mater.* **2020**, *54*, 3731–3741. [[CrossRef](#)]
35. Khammassi, S.; Tarfaoui, M.; Qureshi, Y.; Benyahia, H. Mechanical properties of graphene nanoplatelets reinforced epikote 828 under dynamic compression. *Mech. Mater.* **2021**, *158*, 103873. [[CrossRef](#)]
36. Valášková, M.; Hundáková, M.; Kutláková, K.M.; Seidlerová, J.; Čapková, P.; Pazdziora, E.; Matějová, K.; Heřmánek, M.; Klemm, V.; Rafaja, D. Preparation and characterization of antibacterial silver/vermiculites and silver/montmorillonites. *Geochim. Cosmochim. Acta* **2010**, *74*, 6287–6300. [[CrossRef](#)]

37. Plachá, D.; Kovář, P.; Vaněk, J.; Mikeska, M.; Škrlová, K.; Dutko, O.; Řeháčková, L.; Slabotínský, J. Adsorption of nerve Agent simulants onto vermiculite structure: Experiments and modelling. *J. Hazard. Mater.* **2020**, *382*, 121001. [[CrossRef](#)]
38. Plachá, D.; Jampilek, J. Graphenic materials for biomedical applications. *Nanomaterials* **2019**, *9*, 1758. [[CrossRef](#)]
39. Plachá, D.; Martynková, G.S.; Rummeli, M.H. Variations in the sorptive properties of organovermiculites modified with hexadecyltrimethylammonium and hexadecylpyridinium cations. *J. Sci. Conf. Proc.* **2010**, *2*, 36–41. [[CrossRef](#)]
40. Škrlová, K.; Holíšová, V.; Mikeska, M.; Rybková, Z.; Malachová, K.; Martynková, G.S.; Plachá, D. Polylactide composites suitable for medical devices. *J. Nanosci. Nanotechnol.* **2019**, *19*, 2506–2513. [[CrossRef](#)]
41. Ahmed, J.; Arfat, Y.A.; Castro-Aguirre, E.; Auras, R. Mechanical, structural and thermal properties of Ag–Cu and ZnO reinforced polylactide nanocomposite films. *Int. J. Biol. Macromol.* **2016**, *86*, 885–892. [[CrossRef](#)]
42. Kanmani, P.; Rhim, J.-W. Physical, mechanical and antimicrobial properties of gelatin based active nanocomposite films containing AgNPs and nanoclay. *Food Hydrocoll.* **2014**, *35*, 644–652. [[CrossRef](#)]
43. Venkatesham, M.; Ayodhya, D.; Madhusudhan, A.; Santoshi Kumari, A.; Veerabhadram, G.; Girija Mangatayaru, K. A novel green synthesis of silver nanoparticles using gum karaya: Characterization, antimicrobial and catalytic activity studies. *J. Clust. Sci.* **2014**, *25*, 409–422. [[CrossRef](#)]
44. Zhang, K.; Xu, J.; Wang, R.; Chen, H. Microwave-assisted Synthesis of Polylactide acid/vermiculite Nanocomposites via In-situ Polymerization. *Polym. Mater. Sci. Eng* **2009**, *25*, 162–164.
45. Ye, H.; Hou, K.; Zhou, Q. Improve the thermal and mechanical properties of poly(L-lactide) by forming nanocomposites with pristine vermiculite. *Chin. J. Polym. Sci.* **2016**, *34*, 1–12. [[CrossRef](#)]
46. Belaid, H.; NAgarajan, S.; Teyssier, C.; Barou, C.; Barés, J.; Balme, S.; Garay, H.; Huon, V.; Cornu, D.; Cavailles, V.; et al. Development of new biocompatible 3D printed graphene oxide-based scaffolds. *Mater. Sci. Eng. C* **2020**, *110*, 110595. [[CrossRef](#)]
47. Pinto, A.M.; Moreira, S.; Gonçalves, I.C.; Gama, F.M.; Mendes, A.M.; MAgalhães, F.D. Biocompatibility of poly(lactic acid) with incorporated graphene-based materials. *Colloids Surf. B Biointerfaces* **2013**, *104*, 229–238. [[CrossRef](#)] [[PubMed](#)]
48. Pinto, A.M.; Cabral, J.; Tanaka, D.A.P.; Mendes, A.M.; MAgalhães, F.D. Effect of incorporation of graphene oxide and graphene nanoplatelets on mechanical and gas permeability properties of poly(lactic acid) films. *Polym. Int.* **2013**, *62*, 33–40. [[CrossRef](#)]
49. Kankala, R.K.; Zhu, K.; Sun, X.-N.; Liu, C.-G.; Wang, S.-B.; Chen, A.-Z. Cardiac Tissue Engineering on the Nanoscale. *ACS Biomater. Sci. Eng.* **2018**, *4*, 800–818. [[CrossRef](#)]
50. Nanda, S.S.; Papaefthymiou, G.C.; Yi, D.K. Functionalization of Graphene Oxide and its Biomedical Applications. *Crit. Rev. Solid State Mater. Sci.* **2015**, *40*, 291–315. [[CrossRef](#)]
51. PapAgeorgiou, D.G.; Li, Z.; Liu, M.; Kinloch, I.A.; Young, R.J. Mechanisms of mechanical reinforcement by graphene and carbon nanotubes in polymer nanocomposites. *Nanoscale* **2020**, *12*, 2228–2267. [[CrossRef](#)]
52. El Moumen, A.; Tarfaoui, M.; Lafdi, K. Mechanical characterization of carbon nanotubes based polymer composites using indentation tests. *Compos. Part B Eng.* **2017**, *114*, 1–7. [[CrossRef](#)]
53. Wright-Charlesworth, D.D.; Miller, D.M.; Miskioglu, I.; King, J.A. Nanoindentation of injection molded PLA and self-reinforced composite PLA after in vitro conditioning for three months. *J. Biomed. Mater. Res. Part A* **2005**, *74*, 388–396. [[CrossRef](#)] [[PubMed](#)]
54. Voyiadjis, G.Z.; Samadi-Dooki, A.; Malekmoie, L. Nanoindentation of high performance semicrystalline polymers: A case study on PEEK. *Polym. Test.* **2017**, *61*, 57–64. [[CrossRef](#)]
55. Muzyka, R.; Kwoka, M.; Smedowski, Ł.; Díez, N.; Gryglewicz, G. Oxidation of graphite by different modified Hummers methods. *New Carbon Mater.* **2017**, *32*, 15–20. [[CrossRef](#)]
56. Plachá, D.; Martynková, G.S.; Rummeli, M.H. Preparation of organovermiculites using HDTMA: Structure and sorptive properties using naphthalene. *J. Colloid Interface Sci.* **2008**, *327*, 341–347. [[CrossRef](#)] [[PubMed](#)]
57. Tarfaoui, M.; Lafdi, K.; Beloufa, I.; Daloia, D.; Muhsan, A. Effect of graphene nano-additives on the local mechanical behavior of derived polymer nanocomposites. *Polymers* **2018**, *10*, 667. [[CrossRef](#)]